Arsenic incorporation in pyrite at ambient temperature at both tetrahedral S-I and octahedral Fe+II sites: evidence from EXAFS-DFT analysis

Pierre Le Pape, Marc Blanchard, Jessica Brest, Jean-Claude Boulliard, Maya Ikogou, Lucie Stetten, Shuaitao Wang, Gautier Landrot, Guillaume Morin

Arsenic incorporation in pyrite at ambient temperature at both tetrahedral S^{-I} and octahedral Fe^{+II} sites: evidence from EXAFS-DFT analysis

Pierre Le Pape[1*], Marc Blanchard[1], Jessica Brest[1], Jean-Claude Boulliard[1], Maya Ikogou[1], Lucie Stetten[1], Shuaitao Wang[1], Gautier Landrot[2], and Guillaume Morin[1]

[1] Institut de Minéralogie, de Physique des Matériaux et de Cosmochimie (IMPMC), UMR CNRS 7590, UPMC-IRD-MNHN, Sorbonne Universités, Campus Jussieu, 4 place Jussieu, 75252 Paris cedex 05, France

[2] Synchrotron SOLEIL, F-91192 Gif Sur Yvette, France

*Corresponding Author: Pierre Le Pape

pierrelp.hm@gmail.com

Submitted to *Environmental Science & Technology*

ABSTRACT

Pyrite is an ubiquitous mineral in reducing environments, and is well-known to incorporate trace elements such as Co, Ni, Se, Au and commonly arsenic. Indeed, As-bearing pyrite is observed in a wide variety of sedimentary environments, making it a major sink for this toxic metalloid. Based on the observation of natural hydrothermal pyrites, As^{-I} is usually assigned to the occupation of tetrahedral S sites, with the same oxidation state as in arsenopyrite (FeAsS), even if rare occurrences of As^{III} or As^{II} are reported. However, the modes of As incorporation into pyrite during its crystallization in low-temperature diagenetic conditions are not elucidated yet since arsenic acts as an inhibitor for pyrite nucleation at ambient temperature. Here, we bring evidence from X-ray absorption spectroscopy for $As^{II,III}$ incorporation into pyrite at octahedral Fe^{II} sites and to As^{-I} at tetrahedral S sites during crystallization at ambient temperature. Extended X-Ray absorption fine structure (EXAFS) spectra of these As-bearing pyrites are explained by local structure models obtained using density functional theory (DFT), assuming incorporation of As at the Fe and S sites as well as local clustering of arsenic. Such observation of As^{-I} incorporation at ambient temperature may help understanding the early formation of authigenic arsenian pyrite in subsurface sediments. Moreover, evidence for $As^{II,III}$ for Fe substitution in our synthetic samples questions both the possible occurrence and geochemical reactivity of such type of As-bearing pyrites in low-temperature subsurface environments.

Keywords: As-bearing pyrite, early diagenesis, arsenic sulfides, EXAFS spectroscopy, speciation, density functional theory, oxidation state.

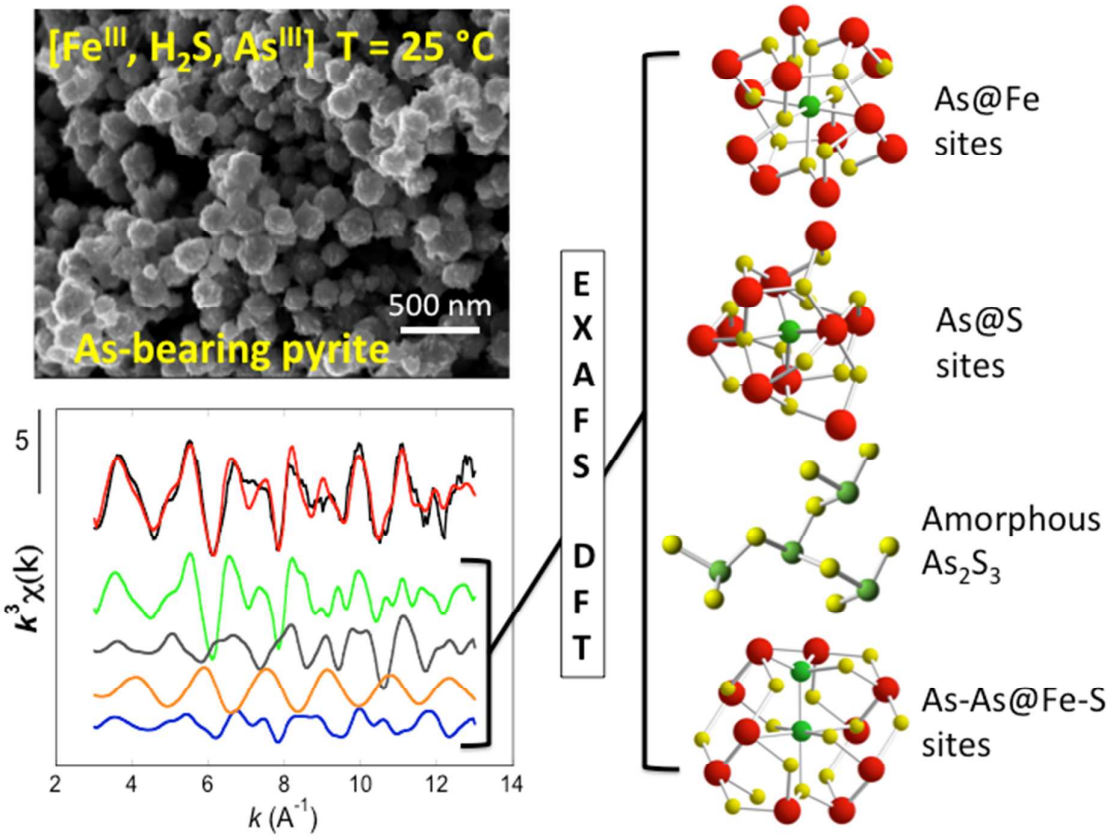
[Fe^{III}, H_2S, As^{III}] T = 25 °C
500 nm
As-bearing pyrite
5
$k^3\chi(k)$
2
4
6
8
10
12
14
k (A^{-1})
EXAFS DFT
As@Fe sites
As@S sites
Amorphous As_2S_3
As-As@Fe-S sites

TOC Art

INTRODUCTION

Arsenic substituted pyrite, known as "arsenian pyrite" is a common mineral occurring in many environments at the Earth's surface. The presence of this mineral has recently been reported in peat samples from Switzerland soils[1] and from sediments of the Mekong delta[2, 3], where it could act as a sink for arsenic, a toxic metalloid, under anoxic conditions. Arsenian pyrite has been also reported to occur in coal samples[4], in alluvial aquifer sediments[5-12], and in salt marsh sediments[13]. The crystal-chemistry of arsenian pyrite has been extensively studied as this mineral is a common host for economically valuable metals such as gold or selenium[14-20].

Arsenic distribution and speciation in natural arsenian pyrite has been experimentally studied using electron microscopy and X-ray absorption spectroscopy[21, 16, 17, 19], revealing that As substitutes for S in the pyrite structure by forming the As-S dianion group with the As^{-I} oxidation state, as also known for arsenopyrite[22]. Accordingly, first-principles and Monte Carlo calculations[23, 24] predicted that As most likely substitutes for tetrahedral S^{-I} in pyrite up to 6-10 wt%. However, XPS and XANES spectroscopic evidences for the presence of As^{III} or As^{II} have also been reported for both natural and synthetic hydrothermal pyrites[25, 26].

In As-contaminated environments such as floodplain deposits or peat soils, arsenian pyrite stands as a major host for As[1, 2, 10]. However, it generally occurs in mixture with other As species, making it difficult to evaluate its geochemical reactivity. In addition, mechanisms of As incorporation into pyrite during early diagenesis remain unclear since arsenian pyrite is particularly difficult to synthesize at ambient temperature in the laboratory. Indeed, the presence of dissolved As^{III} inhibits pyrite nucleation at ambient temperature[27], and sorption experiments of As^{III} on iron sulfides have shown the involvement of complex thio-As intermediates that are difficult to observe and characterize[28-32]. Thus, information related to pyrite formation in the presence of As at ambient temperature are scarce, and the few studies reporting this finding[33, 34] are supported by the monitoring of As concentrations in solution or

by energy dispersive X-Ray micro-analyzes, which do not unambiguously certify that As was incorporated in the crystal structure. In the present study, we thus investigated the modes of arsenic incorporation in pyrite at low temperature in order to elucidate the mechanisms that control As geochemistry in early diagenetic processes. For this purpose, we successfully synthesized nanosized pyrites at ambient temperature in presence of dissolved As^{III}. By comparison with the local atomic structure of As-bearing pyrites modeled using Density Functional Theory (DFT), we bring X-Ray absorption spectroscopy fine structure (EXAFS) spectroscopic evidence for As incorporation into the pyrite structure in both tetrahedral and octahedral coordinations, with a significant spectral signature from octahedrally coordinated $As^{II,III}$.

MATERIALS AND METHODS

Reference mineral samples. Reference As-bearing sulfides minerals were provided by the UPMC mineral collection, namely crystalline orpiment (As_2S_3), crystalline realgar (AsS), arsenopyrite (FeAsS), löllingite ($FeAs_2$), and arsenian pyrite from the Trepça mine. Rietveld refinement of the XRD powder patterns as well as Rietveld refined parameters for these minerals are reported in Fig. S1 and Table S1, respectively. The other As-bearing sulfides used in this study, *i.e.* amorphous orpiment (am_As_2S_3), As^{III}-sorbed pyrite and nanosized As-bearing pyrites were synthesized according to the following protocols. Amorphous orpiment (am-As_2S_3) was precipitated by progressively adding concentrated HCl to a solution containing As^{III} (0.1 M, $NaAsO_2$) and dissolved sulfide (0.625 M, Na_2S). The orange-yellow color precipitate was centrifugated and washed three times with degassed milli-Q water before being dried under vacuum in the anoxic chamber. As^{III} sorption on synthetic pyrite was obtained using As-free nanosized pyrite synthesized at ambient temperature by adapting the protocol initially described in Wei and Osseo-Asare[35] and adapted by Noel et al.[36] for Ni-pyrite. For the sorption experiment, 57 mg of pure nanosized synthetic As-free pyrite dried

under vacuum in Ar atmosphere was reacted with 101 µL of a 0.1 M As^{III} solution in 5 mL of degassed water at pH 6 during 48 hours. The pyrite powder was then recovered by centrifugation and dried under vacuum in the anoxic chamber.

Synthesis of As-bearing pyrite. The synthesis was adapted from the protocol described in Noel et al.[36] for Ni-pyrite. All experiments were achieved in a Jacomex® anoxic chamber under argon atmosphere, and using degassed O_2-free water. Briefly, an appropriate volume of a 0.1 M $NaAsO_2$ solution was added to a 0.625 M $FeCl_3$-$7H_2O$ solution before mixing with a 0.625 M Na_2S-$9H_2O$ solution giving a total volume of 10 mL for 110°C samples and 50 mL for 25°C samples. The glass vials were sealed with butyl rubber stopper and aluminum cap with a bar magnet inside. For the 25°C ambient temperature experiments, batch were gently stirred throughout the synthesis. For the 110°C experiments, batch were kept at 110° C in an oven for 7 days. In the following sections, individual samples are referred to as $FeS_{2-x}As_x$_T where x was defined according to the total As introduced in batch experiments and T was the synthesis temperature in Celsius degrees (°C). Table S2 summarizes the conditions for each of the four As-bearing pyrites synthesized for this study. Rietveld refinement of the XRD powder patterns for the synthetic As-bearing pyrites (Fig. S2 and Table S3) showed that the synthetic samples used in this study are crystalline, and consisted of pure pyrite with minor amounts of goethite and/or marcasite in the samples synthesized at 110°C. Scanning electron microscopy observations showed that the size of the pyrite particles ranged from 0.2 to 2 µm and energy dispersive X-ray spectroscopy indicated the presence of iron, sulfur and arsenic with a stoichiometry close to FeS_2 (Fig. S3).

X-Ray absorption spectroscopy (XAS) data collection. As K-edge X-ray absorption spectra were collected at 10-15 K on the bending magnet SAMBA beamline (SOLEIL, Saint-Aubin, France) using a Si(220) double-crystal monochromator, equipped with dynamic sagittal

focusing of the second crystal. To preserve the oxidation state of As during these analyses, all samples were prepared and mounted on the cryostat sample rod in an anoxic chamber next to the beamline and transferred in a liquid nitrogen bath before being quickly introduced into the He-cryostat. Reference As-sulfide minerals data were collected in transmission mode. The synthetic As-bearing pyrite samples, the arsenian pyrite sample from Trepça and the As^{III}-sorbed pyrite sample were analyzed in fluorescence detection mode using to a 30-elements Ge detector and filtering the background fluorescence signal from the Fe emission lines with Al foils. The incident beam energy was calibrated by setting to 11947 eV the energy position of the absorption maximum in the L_{III}-edge of an Au foil recorded in double-transmission setup. The absorption maximum of As^{III}-S (*e.g.* orpiment-As_2S_3) thus occurs at 11869.5 eV. Between 2 and 10 scans were recorded for both the model compounds and the samples depending on As concentrations. Scans were averaged, normalized and background subtracted using the Athena Software[37] with E_0 set at 11868 eV. Normalized X-ray absorption near edge structure (XANES) spectra were obtained by fitting a linear function to the pre-edge region (E_0-E = 40-250 eV) and a second-order polynomial to the post-edge region (E-E_0 = 150-1000 eV). Extended X-ray Absorption fine structure (EXAFS) data were background subtracted over the 0-13 $Å^{-1}$ *k*-range using the *autobk* algorithm. No clamps were fixed on the spline curve generated.

Extended X-ray absorption fine structure (EXAFS) and X-ray absorption near-edge structure (XANES) data analysis. EXAFS data of the reference As-sulfide minerals were interpreted by comparison with theoretical spectra calculated *ab initio* using the Feff8.1 code[38]. Crystal structures data for these calculations were taken from Mullen and Nowacki[39], Hejny et al.[40], Bindi et al.[41], and Kjekshus et al.[42] for orpiment, realgar, arsenopyrite and löllingite respectively. EXAFS data of the synthetic As-bearing pyrites were interpreted by Linear combination fitting (LCF) using experimental as well as theoretical spectra as fitting

components. These latter were calculated *ab initio* using the Feff8.1 code[38], on the basis of atomic clusters obtained from DTF calculations detailed thereafter. For both reference compounds and DFT-clusters, Feff8.1 *ab initio* calculations of amplitude and phase-shift functions as well as mean-free-path parameters were calculated for 355-958 single and multiple scattering paths (nleg = 8) over a cluster radius of 10 Å. An overall Debye-Waller parameter (σ□, and a threshold energy shift (ΔE_0) parameter were refined to match the experimental EXAFS spectra. The (S_0^2) parameter was fixed to 1.

The EXAFS spectrum of the As^{III}-sorbed pyrite was interpreted using a classical shell-by-shell fitting procedure with phase-shift and amplitude functions for As-O, As-S and As-Fe scattering paths taken from the structure of tooleite[43] and arsenopyrite[41], respectively (Fig. S4 and Table S4). XANES spectra were analyzed using a LCF procedure (Fig. S5 and Table S5), using experimental spectra of our reference As-sulfide minerals as fitting components. As^{III}-sorbed ferrihydrite was considered as additional component as a proxy of the As^{III}-O local As environment. Details about this sample can be found in Wang et al.[44].

DFT modeling of As-bearing pyrites. Four periodic models of As-bearing pyrites were built in a 2×2×2 pyrite supercell (96 atoms). Two models correspond to the substitution of one As atom for either an S atom (structural formula: $Fe_{32}S_{63}As$; As@S model) or one Fe atom ($Fe_{31}AsS_{64}$; As@Fe model). The two other models involve an AsAs pair substituting for either a FeS pair ($Fe_{31}AsS_{63}As$; As-As@Fe-S model) or an SS pair ($Fe_{32}S_{62}As_2$; As-As@S-S model). A reference FeS_2 pyrite structure was also computed. Structural relaxations were performed within the density functional theory (DFT) framework, using the PWscf code of the Quantum ESPRESSO package[45] (http://www.quantum-espresso.org). The ionic core of iron, sulfur and arsenic were described by ultra-soft pseudopotentials from the GBRV library[46]. The incorporation of an arsenic atom into diamagnetic FeS_2 pyrite involves the presence of unpaired electrons, requiring spin-polarized calculations that were conducted using the

generalized gradient approximation (GGA) to the exchange-correlation functional with the PBE parameterization[47]. The electronic wave-functions and charge density were expanded in plane-waves with 40 and 480 Ry cutoffs, respectively, corresponding to a convergence of the total energy better than 1 mRy/atom. The Brillouin zone sampling was restricted to a single *k*-point (Γ-point), which is appropriate to treat such systems with large unit-cell. Structural properties of the optimized models are presented in Table 1.

	Exp. [a]	$Fe_{32}S_{64}$	$Fe_{32}S_{63}As$ (As@S)	$Fe_{31}AsS_{64}$ (As@Fe)	$Fe_{31}AsS_{63}As$ (As-As@Fe-S)	$Fe_{32}S_{62}As_2$ (As-As@S-S)
a_0	5.416	5.406	5.414	5.422	5.425	5.421
S-S	2.158	2.203	2.202-2.231	2.230-2.251	2.229-2.244	2.203-2.227
As-S	-	-	2.288	2.463	2.281-2.452	-
Fe-S	2.264	2.254	2.213-2.272	2.182-2.272	2.172-2.286	2.214-2.268
Fe-As	-	-	2.333	-	2.257-2.262	2.317
As-As	-	-	-	-	2.466	2.445

[a] Brostigen and Kjekshus[48]

Table 1. *Calculated unit-cell parameter (a_0) and interatomic distances (in Å) for pyrite and As-bearing pyrites. Four models were optimized using DFT: As substituting for S (A@S), As substituting for Fe (As@Fe), As-As pair substituting for Fe-S pair (As-As@Fe-S), As-As pair substituting for S-S pair (As-As@S-S).*

RESULTS AND DISCUSSION

Arsenic speciation in reference minerals of the As-Fe-S system. In Earth's surface environments such as soils, waters and sediments, arsenic is encountered in the As^V and As^{III} oxidation states when it is associated with oxygen ligands. In sulfidic environments, As^V is generally reduced to As^{III} and the high affinity of As for sulfur ligands leads to the formation of As-bearing sulfides. These minerals can be arsenic sulfides such as orpiment (As_2S_3) and realgar (AsS), iron arsenic sulfides such as arsenopyrite (FeAsS), as well as arsenides as löllingite ($FeAs_2$). They can form either in hydrothermal or in low-temperature conditions and can incorporate As under various oxidation states.

The energy positions of the white lines in the arsenic K-edge XANES spectra allow to discriminate the oxidation states of arsenic in these minerals: As^{III} in orpiment, As^{II} in realgar, and As^{-I} in arsenopyrite and löllingite (Fig. 1). Thus, arsenic occurs under its most reduced oxidation state (As^{-I}) when it is associated with iron in the structure of sulfide minerals.

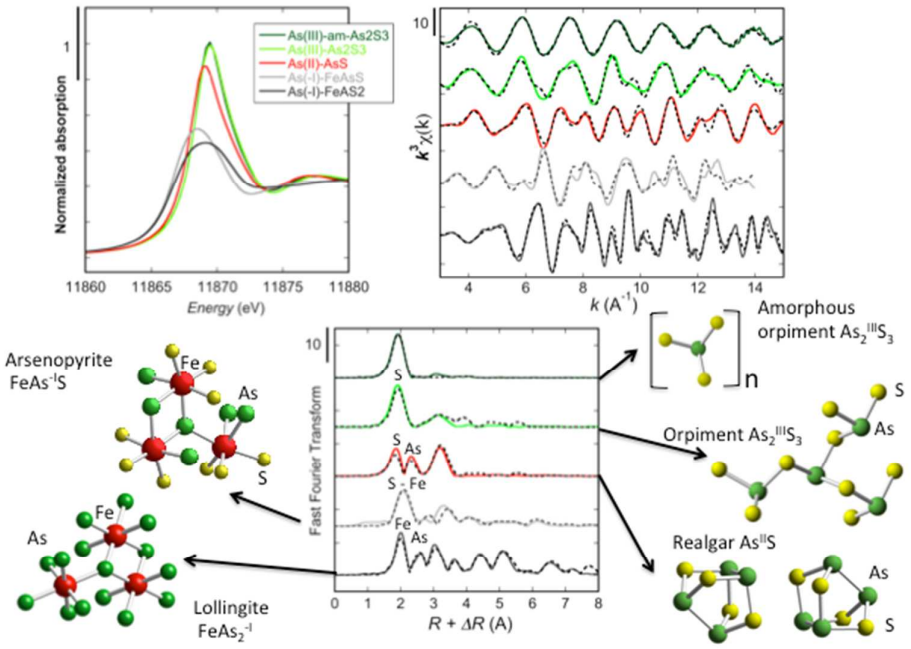

Figure 1. *As K-edge XANES and EXAFS spectra with their Fast Fourier transforms for reference As-bearing sulfides. Corresponding local structures around arsenic are drawn on the right panel. Experimental and Feff8.1 calculated curves are displayed as solid and dotted lines, respectively. Adjustment parameters and crystallographic data used for the Feff8.1 ab initio calculations are reported in Table S6. Rietveld refinement of the XRD powder patterns as well as Rietveld refined parameters for these minerals are reported in Fig. S1 and Table S1, respectively.*

The local structure around arsenic in our series of natural reference As-sulfide minerals was probed by analyzing their As K-edge EXAFS spectra. *Ab initio* Feff8.1 calculation of these spectra attests that the local environment around As in these minerals is consistent with their reported crystal structures (Fig. 1 and Table S6). The coordination geometry of the As atom in these minerals is displayed in Fig. 1 together with the Fast Fourier transform magnitudes (FFT) of the EXAFS spectra. For orpiment, the first peak in the FFT magnitude stands for three S neighbors at 2.27-2.29 Å, whereas in realgar, two peaks are observed, corresponding to two S atoms at 2.22-2.23 Å and one As atom at 2.56 Å. In stoichiometric monoclinic

239 arsenopyrite, the first peak in the FFT corresponds to the backscattering signal of 3 Fe atoms
240 at 2.37, 2.40, and 2.41 Å and 1 S atom at 2.37 Å. In löllingite, the first peak in the FFT is
241 related to three Fe neighbors at 2.36-2.38 Å. To summarize, in these As-bearing sulfides, As
242 is coodinated to three atoms, and the shortest distance is observed for As-S, followed by As-
243 Fe and finally As-As.
244
245 **Arsenic speciation in a natural hydrothermal arsenian pyrite.** To examine the mode of
246 incorporation of arsenic in the natural arsenian pyrite and in the synthetic As-bearing pyrites
247 prepared for the present study, we have compared EXAFS data at the As K-edge of the
248 samples with theoretical spectra calculated using Feff8.1. These calculations were performed
249 on the basis of atomic clusters that were extracted from DFT simulations (Table 1). Using the
250 DFT optimized atomic coordinates for these two models, phase-shift and amplitude functions
251 corresponding to single and multiple scattering paths around the central As atom were
252 calculated with the Feff8.1 code and were then used to calculate the corresponding As K-edge
253 EXAFS spectra to be compared with experimental data (Table S7 and Fig. S6).
254 The experimental As K-edge EXAFS spectrum of our natural reference arsenian pyrite
255 sample from Trepça well matched the spectrum calculated assuming the cluster in which As
256 substitutes for S in the pyrite structure (Fig. 2). Corresponding As-neighbors distances up to 5
257 Å are reported in Table S7. Altogether, XANES and EXAFS results obtained for the arsenian
258 pyrite from Trepça demonstrate that, in this natural pyrite originating from a hydrothermal
259 deposit, arsenic mainly occurs as As^{-I} occupying the tetrahedral S^{-I} site.

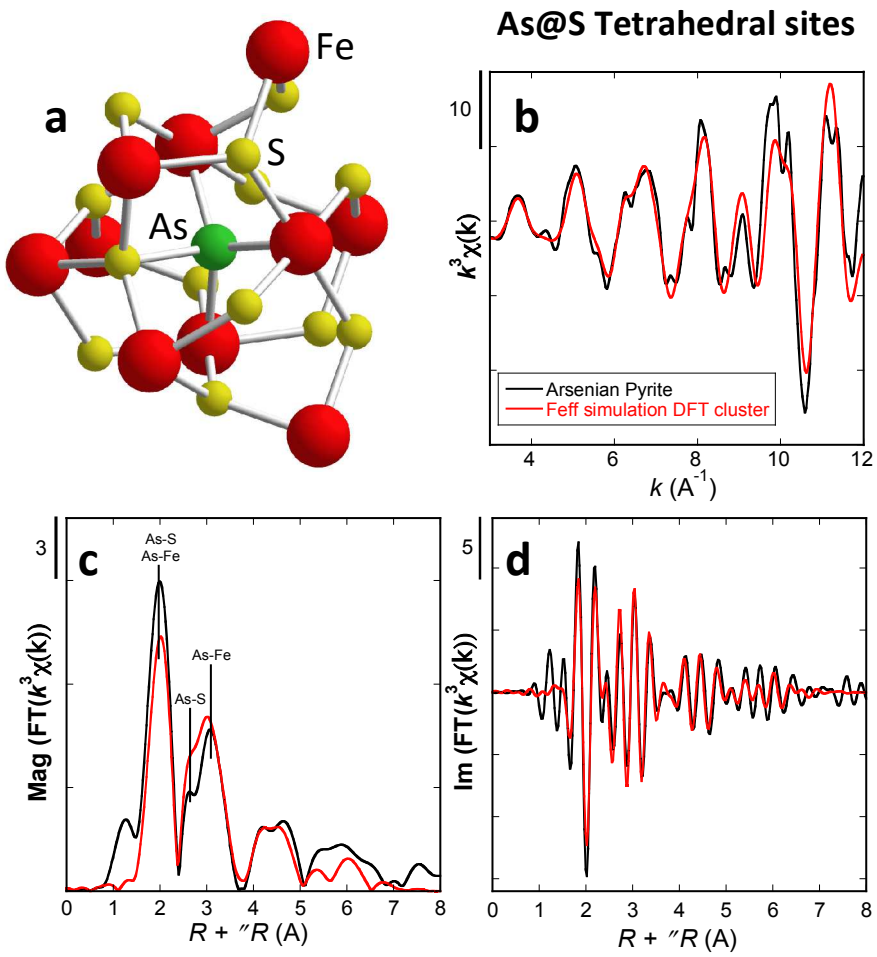

Figure 2. *As K-edge EXAFS analysis of hydrothermal arsenian pyrite from Trepça. (a) Cluster of atoms derived from DFT calculation with an As atom substituting for S at tetrahedral sites (As@S). (b) Experimental EXAFS spectrum (black curve), and ab initio Feff8.1 calculated spectrum using the As@S pyrite cluster simulated by DFT (red curve, Table 1). (c) Magnitude (Mag (FT($k^3\chi(k)$))) and (d) imaginary part (Im (FT($k^3\chi(k)$))) of the Fast Fourier Transform of EXAFS signal uncorrected from phase shift for both experimental and calculated EXAFS spectra. Only a threshold energy shift and an overall Debye-Waller parameter were refined (Table S7).*

Although it is generally assumed that As substitutes for S in the pyrite structure[17, 21], only one study[17] has directly analyzed the atomic environment around As in arsenian pyrite (distances of As neighbors based on shell-by-shell fits until 3.5 Å around As) on the basis of As K-edge EXAFS analysis. These authors however reported the presence of an As-As path at a distance of 3.17 Å, thus suggesting that As atoms could be locally clustered in arsenian pyrite. In the present study, there was no need to consider other As atoms around the As absorber in the As@S cluster used for *ab initio* Feff8.1 calculation to successfully reproduce the

277 experimental EXAFS spectrum of the Trepça sample (Fig. 2 and Table S7). Since this latter
278 spectrum does not differ significantly from that of Savage et al.[17], the difference in the
279 interpretation of these spectra is possibly due to the fact that our DFT models of As@S pyrite
280 better consider the local relaxation of pyrite structure around As.
281
282 **Arsenic incorporation and speciation in pyrite synthesized at ambient temperature.**
283 Although XRD, SEM-EDXS as well as Fe K-edge analyses showed that our synthetic pyrite
284 samples consist of pure crystalline pyrite (Fig. S2, Table S3, Fig. S3, Fig. S7 and Table S8),
285 the As K-edge EXAFS spectrum of sample $FeS_{1.99}As_{0.01}$_25 significantly differs from that of
286 our natural reference sample of arsenian pyrite from Trepça (Fig. 3), and subsequently from
287 the As@S spectrum calculated with a DFT-derived cluster, in which the central As atom
288 substitutes for S at the tetrahedral site (Fig. S6B).
289 Interestingly, the experimental As K-edge EXAFS spectrum of this synthetic pyrite sample is
290 in-phase with our As@Fe DFT simulated cluster in which As replaces Fe at the octahedral
291 site in the pyrite structure (Fig. S6A). Indeed, the specific long distances of 2.46 Å for first S
292 neighbors and 3.85 Å for second Fe neighbors observed by EXAFS are similar to the As-S
293 and As-Fe distances obtained from the DFT cluster (Table 1 and Table S7). In comparison,
294 none of these distances are observed in the As-sulfide mineral references (Fig. 1 and Table
295 S6). However, the amplitude of the experimental EXAFS spectrum is significantly lower than
296 the calculated one, which could be attributed to out-of-phase cancellation of the EXAFS
297 signal, due either to site distortion or to interferences with EXAFS signals from other local
298 environments of arsenic in the sample. In order to evaluate the effect of site distortion, off-
299 centering of the As atom in the octahedral site was tested by shifting the As atom along the *c*
300 axis from the central position obtained from the DFT cluster (Fig. S8). A slight displacement
301 of the As atom decreased the amplitude of the calculated EXAFS spectrum (Fig. S8B),
302 indicating that slight As off-centering in the Fe sites could possibly occur in our sample.

303 Strong off-centering of the As atom results in a better match in EXAFS amplitude but fails at
304 reproducing the EXAFS spectrum shape (Fig S8C), which suggests that other types of local
305 environment for As are present in the sample.
306 Indeed, out-of-phase cancellation of EXAFS signals from distinct As local environments in
307 our synthetic pyrite sample ($FeS_{1.99}As_{0.01}$_25) is supported by the amplitude reduction
308 obtained when adding a contribution of As@S sites (25%) to that of As@Fe sites (75%),
309 which furthermore improves the matching between the calculated and experimental EXAFS
310 spectra (Fig. S9B). Moreover, adding a contribution of amorphous-As_2S_3, which is consistent
311 with precipitation from As^{III} and H_2S in the synthesis medium[49, 50] significantly improves the
312 matching to the experimental spectrum, even when keeping the sum of the components at
313 100% (Fig. S9C). This good match relies on the fact that the EXAFS signal of As@Fe is out-
314 of-phase with both the signals of As@S and that of am-As_2S_3 (Fig S6). This result shows that
315 the drastic amplitude reduction observed in the As K-edge EXAFS of our synthetic pyrite
316 samples is mainly due to out-of-phase cancellation between EXAFS signals arising from
317 diverse local As environments in our synthetic samples, which include substitution of As at
318 both the Fe and S sites.
319 Additionally, we also tested the possibility of local As clustering in the pyrite structure by
320 simulating EXAFS signal from DFT-derived clusters including As-As atom pairs replacing
321 either Fe-S or S-S pairs in the pyrite structure (Fig. S6 and Table S7), which correspond to
322 models As-As@Fe-S and As-As@S-S in Table 1, respectively. A better agreement between
323 calculations and experimental data is observed when the As-As pair replaces a Fe-S pair than
324 when it replaces a S-S pair (Fig. S6). Interestingly, the EXAFS obtained with an As-As pair
325 better matches the amplitude of the experimental signal than the combination of the EXAFS
326 obtained with As atoms substituting for Fe and S at non adjacent sites (Fig. S6). This is
327 explained by the significant site distortion around As atoms implied by the pair substitution
328 (Table 1), which generates EXAFS dampening due to static disorder around arsenic. Such

result suggests that As clustering likely occurs in our synthetic pyrite samples, which would contribute to the observed lowering of experimental EXAFS amplitude at the As K-edge. However, the calculated signal obtained for As-As pairs substituting for As-Fe pair does not match alone the experimental data (Fig. S6D), which indicates that such As-As clusters occur in addition to the As atoms substituting for Fe and S at non adjacent sites. Indeed, the best match to the experimental EXAFS data of sample $FeS_{1.99}As_{0.01}$_25 is obtained by a linear combination of the calculated spectra of the following components: As@Fe site, As@S site, As-As@Fe-S site, and am-As_2S_3. This best fit is plotted in Fig S9 and Fig. 3 considering the sum of the components normalized to 100% or non-normalized, respectively. The sum of the components of 71 % (Table 2) could be accounted for by assuming an acceptable value of ~0.7 for the S_0^2 attenuation factor[51]. However, we rather interpret this difference to 100% as being due to minor contributions from a variety of other As clustering configurations and of site distortion in the structure of our synthetic As-bearing pyrites. Thus, such complex As site distribution could not be easily modeled using a DFT approach. Nevertheless, comparison of the experimental As-EXAFS data with specific local configurations relaxed using DFT allows demonstrating that As substitutes at both tetrahedral S and octahedral Fe sites during pyrite crystallization at ambient temperature in our experiments (Fig. 3).

Based on XPS measurements on the *3d* orbitals of arsenic performed on a natural hydrothermal pyrite, a study by Deditius et al.[25] brought the evidence that As could naturally occur in pyrite as As^{III}. Another recent study by Qian et al.[26] based on XANES spectroscopy proposed that As^{II} substitutes for Fe in pyrite synthesized under hydrothermal conditions from mixtures of H_2S and magnetite. In this study, XANES-LCF on the $FeS_{1.99}As_{0.01}$_25 sample indicates around ~ 70 % of $As^{II,III}$ (Fig. S5 and Table S5), which is consistent with our EXAFS – DFT analysis that indicates ~ 65 % of As incorporated as $As^{II,III}$ in the pyrite structure. Finally, we bring here the first evidence that As substitutes for Fe during pyrite

crystallization at ambient temperature, *i.e.* in conditions that may be relevant to early diagenesis of sediments.

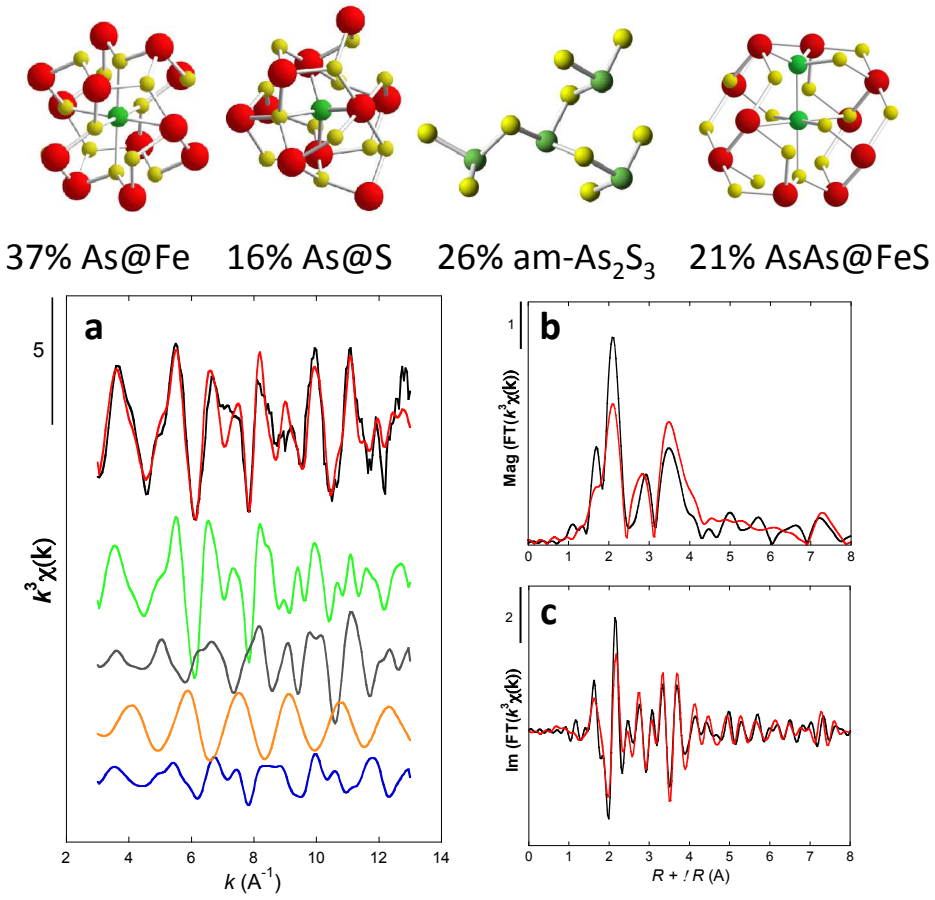

Figure 3. *Linear combination fit (LCF) of the experimental As K-edge EXAFS spectrum of the $FeS_{1.99}As_{0.01}$_25 sample using spectra simulated using the feff8.1 code from atomic clusters calculated using DFT (As@Fe, As@S, As-As@Fe-S, Table 1, Fig S6 and Table S7) and amorphous orpiment (am_As_2S_3, Fig.1 and table S6). (a) EXAFS experimental spectrum (black curve), EXAFS-LCF fit (red curve), and weighted spectra of the fitting components displayed below (Table 2). Fitted proportions of the As species indicated below the atom clusters are normalized to 100% as in Fig. 4 bar diagram. (b) Magnitude (Mag (FT($k^3\chi(k)$))) and (c) imaginary part (Im (FT($k^3\chi(k)$))) of the Fast Fourier Transform of EXAFS signal uncorrected from phase shift for both experimental and simulated EXAFS spectra.*

Arsenic speciation as a function of As/S molar ratio and temperature. To determine arsenic speciation in the synthetic As-bearing pyrites, a linear combination fit (LCF) procedure was applied to reconstruct the experimental EXAFS signals using selected reference EXAFS spectra (Fig. 4 and Table 2). For this purpose, we used as fitting

components the EXAFS spectra of : i) EXAFS-DFT of As@S sites in pyrite (Fig. 2, Fig S6 and Table S7), ii) EXAFS-DFT of As@Fe sites in pyrite (Fig. 3, Fig S6 and Table S7), iii) EXAFS-DFT of As-As@Fe-S sites in pyrite (Fig. 3, Fig S6 and Table S7), iv) amorphous orpiment (Fig. 1, Table S6), and v) As^{III}-sorbed pyrite in which As local environment was determined using a shell-by-shell fitting procedure (Fig. S4, Table S4).

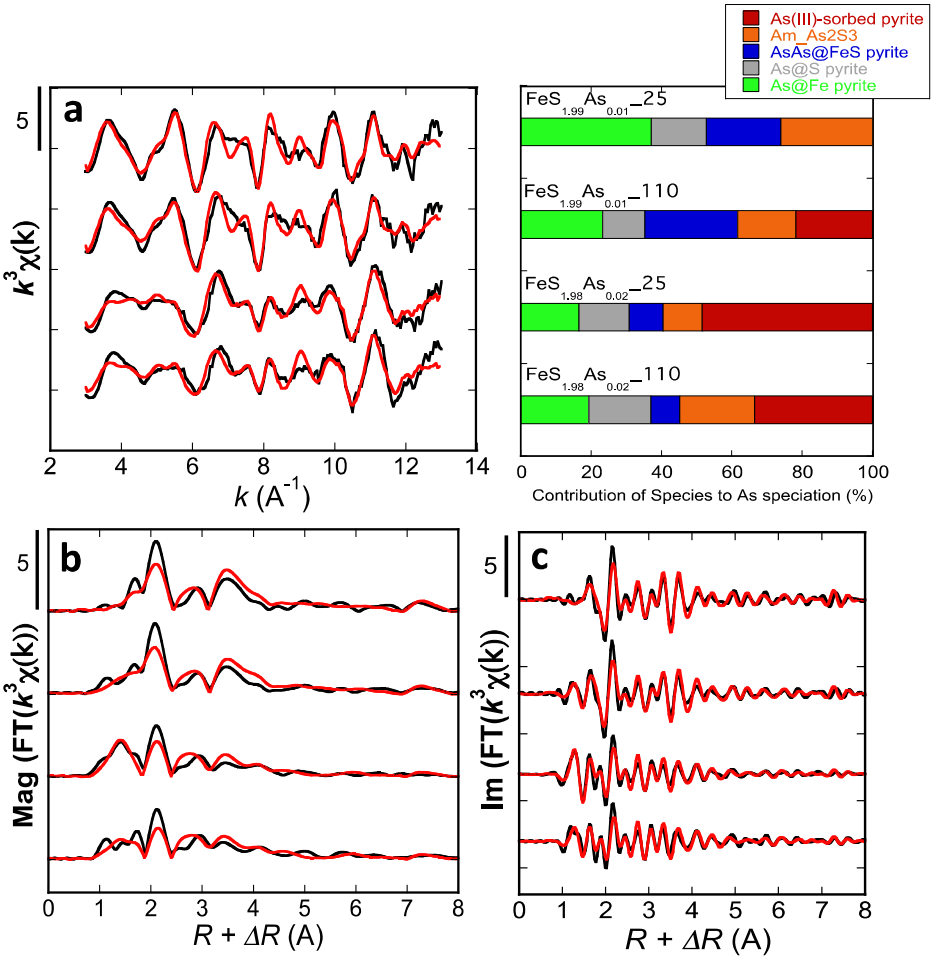

Figure 4. *Linear combination fit of the experimental As K-edge EXAFS spectra of the synthetic As-bearing pyrite samples prepared with two distinct As/S molar ratio and at 25 or 110 °C. (a) EXAFS-LCF with selected fitting components simulated using feff8.1 from atomic clusters obtained from DFT calculations (As@Fe, As@S, As-As@Fe-S), amorphous orpiment, and As^{III}-sorbed pyrite. Proportions of the fitting components with a sum normalized to 100% are displayed in the bar diagram. Non-normalized results and estimators of fit quality are given in Table 2. Magnitude (Mag (FT($k^3\chi(k)$))) and imaginary part (Im (FT($k^3\chi(k)$))) of the Fast Fourier Transform of EXAFS signals uncorrected from phase shift for both experimental and simulated EXAFS spectra are displayed in (b) and (c), respectively.*

	As@Fe	As@S	am_As_2S_3	As-As@Fe-S	As^{III}-sorbed Pyrite	Sum	R_f	χ^2	Red-χ^2
$FeS_{1.99}As_{0.01}$_25	26 (5)	11 (3)	19 (5)	15 (7.5)	-	71	0.19	96	0.49
$FeS_{1.99}As_{0.01}$_110	20 (5)	10 (3)	14 (5)	22 (7)	19 (7)	85	0.19	88	0.45
$FeS_{1.98}As_{0.02}$_25	12 (5)	11 (3)	8 (5)	7 (6)	36 (6)	74	0.19	64	0.33
$FeS_{1.98}As_{0.02}$_110	13 (5)	12 (3)	15 (5)	6 (5)	23 (6)	70	0.26	84	0.43

Table 2. *Results of the linear combination fitting (LCF) procedure applied to As K-edge EXAFS data using EXAFS spectra simulated from DFT structures (As@Fe, As@S, AsAs@FeS, Table 1 and Fig. S6) and EXAFS spectra from reference compounds in which As speciation has been checked by feff8.1 simulation (am_As_2S_3, Fig. 1 and Table S6) and shell-by-shell fitting (AsIII-sorbed pyrite, Fig. S4 and Table S4). LCF were performed within the 3-13 $Å^{-1}$ k-range using the Athena software. Fitted percentages of the fitting component in each sample are reported without normalizing the sum to 100%. R-factor (Rf), chi-square (χ^2) and reduced chi-square (Red-χ^2) are given as classical estimators of the quality of fit. Uncertainties on the fitted values are given in parentheses and refer to 3 sigma obtained with the Athena software.*

For As-bearing pyrite synthesized at low As/S molar ratio, *i.e.*, $FeS_{1.99}As_{0.01}$ stoichiometry, both 25 °C and 110 °C samples exhibit a dominant contribution from As incorporated in the pyrite structure at both Fe and S sites and minor amounts of amorphous As_2S_3 and As^{III}-sorbed pyrite (Fig. 4).

At a higher As/S molar ratio, corresponding to the $FeS_{1.98}As_{0.02}$ stoichiometry, a significant additional contribution of As^{III}-sorbed pyrite is observed, showing that when arsenic concentration is increased in the starting solution, only a fraction of As is able to enter in the crystal lattice of pyrite in the conditions of our synthesis (Fig. 4).

Concerning the proportions of As in the pyrite structure, a relatively stable contribution of As@S site is observed regardless the As/S ratio while larger contributions of both As@Fe and As-As@Fe-S are observed for low As/S ratio. Such difference possibly illustrates slight differences in As site distribution in the pyrite structure.

Contributions of As species to the experimental EXAFS signal are relatively similar at both 25°C and 110 °C synthesis temperatures for a given As/S molar ratio, attesting that the temperature only slightly influences As speciation within the temperature range investigated

here. However, our experiments demonstrate that increasing the temperature significantly accelerate pyrite crystallization since As-bearing pyrites synthesized at 110 °C formed only after 7 days instead of months at ambient temperature (Table S2).

Altogether, these EXAFS-LCF results would indicate that As speciation is most likely driven by the initial concentrations of reactants, *i.e.* As^{III}, Fe^{III} and H_2S in solution and by physico-chemical parameters such as pH. Indeed, reduction of Fe^{III} by H_2S to form FeS_2 *via* the polysulfide pathway implies the production of H^+ [35, 52]. Then, acidification could have an influence on pH-sensitive reaction intermediates involved in As incorporation into pyrite such as thio-As species[28-32].

Arsenic oxidation state in As-bearing pyrite samples. In order to evaluate the proportions of the different oxidation states of arsenic in the As-bearing pyrite samples, LCF of XANES spectra were performed on the experimental XANES spectra using the reference compounds presented in Fig. S5 as fitting components. LCF results indicated that arsenic is mainly present as As^{III}/As^{II} (53-71%) and as As^{-I} (19-36%) in the samples (Fig. S5 and Table S5), which is consistent with As^{III}/As^{II} replacing Fe^{II} and As^{-I} replacing S^{-I} in the pyrite structure, according to our EXAFS results.

The energy position of the white line for the reference As@S arsenian pyrite from Trepça is close to that of arsenopyrite, which is consistent with the presence of As under the As^{-I} oxidation state, in agreement with previous literature[2, 17, 21, 24]. Indeed, it was reported from DFT calculations that it is more energetically favorable to substitute As for S than for Fe in the pyrite structure[24].

LCF of XANES spectra of our synthetic As-bearing pyrite samples revealed that a non-negligible part of As is present as As^{-I}, thus showing that the reduction of As from As^{III} to As^{-I} is not only possible under hydrothermal conditions as in the case of arsenopyrite, but can also occur at ambient temperature. This would finally indicate that crystallization of As@S

443 arsenian pyrite could partly occur during early diagenesis, even if the underlying mechanism
444 of As reduction remains to be elucidated in low temperature systems[25, 28, 29].
445 In addition, a large part of As is incorporated in the form of $As^{II,III}$ into pyrite, form that has
446 been only scarcely detected in pyrites of hydrothermal origin[25, 26]. Here, the pyrite formation
447 pathway involves oxidation of H_2S by Fe^{III} and subsequent reaction of S^0 with FeS, *via* the
448 polysulfide pathway[51]. This route yields more oxidizing conditions than those that could
449 prevail when FeS reacts with $H_2S_{(g)}$[53, 25], and could thus favor the incorporation of $As^{II,III}$
450 (As@Fe) over As^{-I} (As@S) in pyrite.
451
452 **Environmental implications.** This study shows that (i) pyrite can crystallize at ambient
453 temperature from a mixture of dissolved Fe^{III} and H_2S in presence of As^{III}, (ii) As^{III} can be
454 reduced to As^{-I} oxidation state at ambient temperature, As^{-I} being then incorporated into pyrite
455 at the tetrahedral S^{-I} site, (iii) As^{III} is incorporated under a $As^{II,III}$ oxidation state in pyrite
456 synthesized at ambient temperature *via* the polysulfide pathway, with interatomic distances
457 corresponding to the occupation of octahedral Fe sites, and (iv) increasing temperature only
458 slightly affects As speciation but speeds up the crystallization process from a few weeks at
459 ambient temperature to few hours at 110°C. These findings set the basis for a better
460 understanding of the early stages of formation of authigenic arsenian pyrite in shallow
461 sediments and groundwaters at ambient temperature and thus suggest that such phase could
462 represent an active arsenic sink in sub-surface sulfidic environments.
463 The presence of arsenian pyrite was recently evidenced using EXAFS spectroscopy as a main
464 As-bearing mineral in deltaic sediments of Southeast Asia[2, 3]. In these studies, the spectral
465 features observed were consistent with As@S substitution in pyrite, *i.e.* similar to the
466 speciation described by Savage et al.[17] and in Fig. 2. Since As-contaminated sediments
467 represent a source of arsenic to groundwater, determining the origin and fate of such As-
468 bearing pyrites is a major environmental issue. In Lowers et al.[10] as well as in Wang et al.[3],

the presence of arsenic in individual framboids from framboidal pyrites pushes the idea that authigenic formation of arsenian pyrite could occur during early diagenesis. The present study which investigated As incorporation in pyrite at ambient temperature showed that, in addition to As for S substitution, a major fraction of As can be incorporated at the Fe site in the pyrite structure. The EXAFS signature of As@Fe site is out-of-phase with that of As@S site in the structure, which could hinder its detection in mixture with other species in complex arsenic diluted natural samples. However, since $As^{II,III}$ in pyrite has been already detected in natural conditions[25], these findings motivate further investigations to search for the possible presence of such species in subsurface environments in which the polysulfide pyrite formation pathway could occur. In addition, little is known on the long-term evolution of freshly precipitated pyrite particles that were shown here to contain a large proportion of As at the As@Fe site. Although this $As^{II,III}$ component was shown to be preserved in the samples prepared at 110°C over a week time-scale, further studies would be required to evaluate its potential further transformation into other As species under reducing or oxidizing conditions.

Associated content

Supporting information

The supporting information section contains Tables S1-S8 and Figures S1-S9.

Author information

Corresponding author

*Phone: +33 0 1 44 27 42 27

E-mail: pierrelp.hm@gmail.com

Acknowledgements

The authors thank Imene Esteve, as well as Benoit Baptiste and Ludovic Delbes for their technical assistance in the use of SEM-EDXS and XRD facilities of IMPMC.. The staff of the SOLEIL synchrotron, Orsay (France), and in particular Emiliano Fonda, Andrea Zitolo and Guillaume Alizon from the SAMBA beamline group are acknowledged for their technical support during XAS measurements. DFT calculations were performed using HPC resources from GENCI-IDRIS (Grant 2016-i2016041519). This study was partly granted by ANR IngECOST-DMA (ANR-13-ECOT-0009). We thank the anonymous reviewers for their comments and suggestions that help to improve the manuscript.

References

(1) Langner P., Mikutta C., Suess E., Marcus M. A., Kretzschmar R. (2013) Spatial distribution of arsenic in peat studied with microfocused X-ray fluorescence spectrometry and X-ray absorption spectroscopy. Environmental Science and technology 47, 9706-9714.

(2) Stuckey J. W., Schaefer M. V., Kocar B. D., Dittmar J., Lezama Pacheco J., Benner S. G., Fendorf S. (2015) Peat formation concentrates arsenic within sediment deposits of the Mekong delta. Geochimica et Cosmochimica Acta 149, 190-205.

(3) Wang Y., Le Pape P., Morin G., Suvorova E., Bartova B., Asta M., Frutschi M., Ikogou M., Pham V., Vo P., Charlet L., and Bernier-Latmani R. A carbon nanotube-associated arsenic species in Mekong Delta sediments. Abstract 3357 of the 2016 Goldschmidt conference.

(4) Huggins F. E., Huffman G. P. (1996) Modes of occurrence of trace elements in coal from XAFS spectroscopy.

519 (5) Das D., Samanta G., Mandal B. K., Chowdhury T. R., Chanda C. R., Chowdhury P. P.,
520 Basu G. K., chakraborti D. (1996) Arsenic in groundwater in six districts of west
521 Bengal, India. Environmental Geochemistry and Health 18, 5-15.
522 (6) Nickson R., McArthur J., Burgess W., Ahmed K.M., Ravenscroft P., Rahman M. (1998)
523 Arsenic poisoning of Bangladesh groundwater. Nature 395, 338.
524 (7) McArthur J. M., Ravenscroft P., Safiulla S., Thirlwall M. F. (2001) Arsenic in
525 groundwater: Testing pollution mechanisms for sedimentary aquifers in Bangladesh.
526 Water Resources Research 37 (1), 109-117.
527 (8) Kim M-J., Nriagu J., Haack S. (2002) Arsenic species and chemistry in groundwater of
528 southest Michigan. Environmental Pollution 120, 379-390.
529 (9) Polizzotto M. L., Harvey C. F., Sutton S. R., Fendorf S. (2005) Processes conductive to
530 the release and transport of arsenic into aquifers of Bangladesh. Proceedings of the
531 national academy of science of the USA 102 (52), 18819-18823.
532 (10) Lowers H.A., Breit G.N., Foster A.L., Whitney J., Yount J., Uddin M.N., Muneem A.A.
533 (2007) Arsenic incorporation into authigenic pyrite, Bengal Basin sediment,
534 Bangladesh. Geochimica et Cosmochimica Acta 71, 2699–2717.
535 (11) Peters S. C., Burkert L. (2008) The occurrence and geochemistry of arsenic in
536 groundwaters of the Newark basin of Pennsylvania. Applied Geochemistry 23, 85-98.
537 (12) Mango H., Ryan P. (2015) Source of arsenic-bearing pyrite in southwestern Vermont,
538 USA: sulfur isotope evidence. Science of the total environment 505, 1331-1339.
539 (13) Neuman T., Scholz F., Kramar U., Ostermaier M., Rausch N., Berner Z. (2013) Arsenic
540 in framboidal pyrite from recent sediments of a shallow water lagoon of the Baltic sea.
541 Sedimentology 60, 1389-1404.
542 (14) Wells J. D., Mullens T. E. (1973) Gold-bearing arsenian pyrite determined by
543 microprobe analysis, Cortez and Carlin gold mines, Nevada. Economic Geology 68,
544 187-201.

(15) Fleet M. E., Mumin A. H. (1997) Gold-bearing arsenian pyrite and marcasite and arsenopyrite from Carlin Trend gold deposits and laboratory synthesis. American mineralogist 82, 182-193.

(16) Simon G., Huand H., Penner-Hahn J. E., Kesler S. E., Kao L-S. (1999) Oxidation state of gold and arsenic in gold-bearing arsenian pyrite. American Mineralogist 84, 1071-1079.

(17) Savage K. S., Tingle T. N., O'Day P. A., Waychunas G. A., Bird D. K. (2000) Arsenic speciation in pyrite and secondary weathering phases, Mother Lode gold district, Tuolumne county, California. Applied geochemistry 15, 1219-1244.

(18) Reich M., Kesler S. E., Utsunomiya S., Palenik C. S., Chryssoulis S. L., Ewing R. C. (2005) Solubility of gold in arsenian pyrite. Geochimica et Cosmochimica Acta 69 (11), 2781-2796.

(19) Kang M., Bardelli F., Charlet L., Géhin A., Shchukarev A., Chen F., Morel M-C., Ma B., Liu C. (2014) Redox reaction of aqueous selenite with As-rich pyrite from Jiguanshan ore mine (China): Reaction products and pathways. Applied Geochemistry 47, 130-140.

(20) Agangi A., Przybylowicz W., Hofmann A. (2015) Trace element mapping of pyrite from Archean gold deposits - A comparison between PIXE and EPMA. Nuclear instruments and Methods in physics research B 348, 302-306.

(21) Foster A. L., Brown G. E. Jr, Tingle T. N., Parks G. A. (1998) Quantitative arsenic speciation in mine tailings using X-ray absorption spectroscopy. American Mineralogist 83, 553-568.

(22) Nesbitt H. W., Muir I. J., Pratt A. R. (1995) Oxidation of arsenopyrite by air and air-saturated, distilled water, and implications for mechanism of oxidation. Geochimica et Cosmochimica Acta 59 (9), 1773-1786.

570 (23) Reich M., Becker U. (2006) First-principles calculations of the thermodynamic mixing
571 properties of arsenic incorporation into pyrite and marcasite. Chemical Geology 225,
572 278-290.
573 (24) Blanchard M., Alfredsson M., Brodholt J., Wright K., Richard C., Catlow A. (2007)
574 Arsenic incorporation into FeS2 pyrite and its influence on dissolution: a DFT study.
575 Geochimica et Cosmochimica Acta 71, 624-630.
576 (25) Deditius A. P., Utsunomiya S., Renock D., Ewing R. C., Ramana C. V., Becker U.,
577 Kesler S. E. (2008) A proposed new type of arsenian pyrite: composition,
578 nanostructure and geological significance. Geochimica et Cosmochimica Acta 72,
579 2919-2933.
580 (26) Qian G., Brugger J., Testemale D., Skinner W., Pring A. (2013) Formation of As(II)-
581 pyrite during experimental replacement of magnetite under hydrothermal conditions.
582 Geochimica et Cosmochimica Acta 100, 1-10.
583 (27) Wolthers M., Butler I. B., Rickard D. (2007) Influence of arsenic on iron sulfide
584 transformations. Chemical Geology 236, 217-227.
585 (28) Farquhar M. G., Charnock J. M., Livens F. R., Vaughan D. J. (2002) Mechanisms of
586 arsenic uptake from aqueous solution by interaction with goethite, lepidocrocite,
587 mackinawite, and pyrite: an X-ray absorption spectroscopy study. Environmental
588 Science and technology 36, 1757-1762.
589 (29) Bostick B. C., Fendorf S. (2003) Arsenite sorption on troilite (FeS) and pyrite (FeS_2).
590 Geochimica et Cosmochimica Acta 67 (5), 909-921.
591 (30) Gallegos T. J., Hyun S. P., Hayes K. F. (2007) Spectroscopic investigation of the uptake
592 of arsenite from solution by synthetic mackinawite. Environmental Science and
593 Technology 41, 7781-7786.

(31) Burton E. D., Johnston S. G., Planer-Friedrich B. (2013) Coupling of arsenic mobility to sulfur transformations during microbial sulfate reduction in the presence and absence of humic acid. Chemical Geology 343, 12-24.

(32) Couture R-M., Rose J., Kumar N., Mitchell K., Wallschlager D., Van Cappellen P. (2013) Sorption of arsenite, arsenate and thioarsenates to iron oxides and iron sulfides: a kinetic and spectroscopic investigation. Environmental Science and Technology 47, 5652, 5659.

(33) Wolthers M., Butler I. B., Rickard D., Mason P. R. D. (2004) Arsenic uptake by pyrite at ambient environmental conditions: a continuous-flow experiment. American Chemical Society (ACS) Symposium Series 915, 60-76, chapter of book.

(34) Kirk M. F., Roden E. E., Crossey L. J., Brealey A. J., Spilde M. N. (2010) Experimental analysis of arsenic precipitation during microbial sulfate and iron reduction in model aquifer sediment reactors. Geochimica et Cosmochimica Acta 74, 2538-2555.

(35) Wei D., Osseo-Asare K. (1997) Aqueous synthesis of finely divided pyrite particles. Colloids and Surfaces A: Physicochemical and Engineering Aspects 121 (1), 27-36.

(36) Noel V., Morin G., Juillot F., Marchand C., Brest J., Bargar J. R., Munoz M., Marakovic G., Ardo S., Brown G.E. Jr, Ni cycling in mangrove sediments from New Caledonia. Geochimica et Cosmochimica Acta 169, 82-98.

(37) Ravel B. and Newville M. (2005) ATHENA, ARTEMIS, HEPHAESTUS: data analysis for X-ray absorption spec- troscopy using IFEFFIT. J. Synchrotron Rad. 12, 537–541.

(38) Ankudinov A. L., Ravel B., Rehr J. J. and Conradson S. D. (1998) Real-space multiple-scattering calculation and interpretation of X-ray-absorption near-edge structure. Phys. Rev. B 58, 7565– 7576.

(39) Mullen D. J. E., and Nowacki W. (1972) Refinement of the crystal structures of realgar, AsS and orpiment, As2S3. Zeitschrift für Kristallographie - Crystalline Materials 136, 1-6.

620 (40) Hejni C., Sagl R., Tobbens D. M., Miletich R., Wildner M., Nasdala L., Ullrich A., and
621 Balic-Zunic (2012) Crystal-structure properties and the molecular nature of
622 hydrostatically compressed realgar. Phys Chem Minerals 39, 399-412.
623 (41) Bindi L., Moelo Y., Leone P., Suchaud M. (2012) Stoichiometric arsenopyrite, FeAsS,
624 from La Roche-Balue, Quarry, Loire-Atlantique, France: Crystal structure and
625 Mossbauer study. The Canadian Mineralogist 50 (2), 471-479.
626 (42) Kjekshus A., Rakke T., Andresen A. (1974) Compounds of the marcasite type crystal
627 structure. IX. Structural data for $FeAs_2$, FeSe2, NiSb2, and CuSe2. Acta Chemical
628 Scandinavia A28, 996-1000.
629 (43) Morin G., Rousse G. and Elkaim E. (2007) Crystal structure of tooeleite, a new iron
630 arsenite hydroxysulfate relevant of acid mine drainage. Amer. Mineral. 92, 193–197.
631 (44) Wang Y, Morin G., Ona-Nguema G., Menguy N., Juillot F., Aubry E., Guyot F., Calas
632 G., Brown GE (2008) Arsenite sorption at the magnetite-water interface during
633 aqueous precipitation of magnetite: EXAFS evidence for a new arsenite surface
634 complex. Geochimica et Cosmochimica Acta 72 (11), 2573-2586.
635 (45) Giannozzi, P., Baroni, S., Bonini, N., Calandra, M., Car, R., Cavazzoni, C., Ceresoli, D.,
636 Chiarotti, G.L., Cococcioni, M., Dabo, I., Dal Corso, A., de Gironcoli, S., Fabris, S.,
637 Fratesi, G., Gebauer, R., Gerstmann, U., Gougoussis, C., Kokalj, A., Lazzeri, M.,
638 Martin-Samos, L., Marzari, N., Mauri, F., Mazzarello, R., Paolini, S., Pasquarello, A.,
639 Paulatto, L., Sbraccia, C., Scandolo, S., Sclauzero, G., Seitsonen, A.P., Smogunov, A.,
640 Umari, P., and Wentzcovitch, R.M. (2009) Quantum ESPRESSO: a modular and
641 open-source software project for quantum simulations of materials. Journal of Physics:
642 Condensed Matter, 21, 395502.
643 (46) Garrity, K.F., Bennett, J.W., Rabe, K.M., Vanderbilt, D. (2014) Pseudopotentials for
644 high-throuhput DFT calculations. Comput. Mat. Sci. 81, 446-452.

645 (47) Perdew, J.P., Burke, K., and Ernzerhof, M. (1996) Generalized Gradient Approximation
646 Made Simple. Physical Review Letters, 77, 3865–3868.
647 (48) Brostigen, G., Kjekshus, A., (1969) Redetermined crystal structure of FeS_2 (pyrite). Acta
648 Chem. Scand. 23, 2186–2188.
649 (49) O'Day P. A., Vlassopoulos D., Root R., Rivera N. (2004) The influence of sulfur and
650 iron on dissolved arsenic concentrations in the shallow subsurface under changing
651 redox conditions. Proceedings of the National Academy of Science of America 101
652 (38), 13703-13708.
653 (50) Le Pape P., Battaglia-Brunet F., Parmentier M., Joulian C., Gassaud C., Fernandez-Rojo
654 L., Guigner J-M., Ikogou M., Stetten L., Olivi L., Casiot C., Morin G. (2016)
655 Complete removal of arsenic and zinc from a heavily contaminated acid mine
656 drainage *via* an indigenous SRB consortium. Journal of hazardous Materials, in press.
657 (51) Teo B. K. (1986) EXAFS: Basic Principles and Data Analysis. Inorganic Chemistry
658 Concepts 9, Springer-Verlag, Book.
659 (52) Rickard D., Luther G. W. (2007) Chemistry of iron sulfides. Chemical Review 107, 514-
660 562.
661 (53) Rickard D. (1997) Kinetics of pyrite formation by the H_2S oxidation of iron (II)
662 monosulfide in aqueous solutions between 25 and 125 °C: the rate equation.
663 Geochimica et Cosmochimica Acta 61 (1), 115-134.
664